

Construction and Hierarchical Self-Assembly of Multifunctional Coordination Cages with Triangular Metal–Metal-Bonded Units

Zi-En Zhang, Yi-Fan Zhang, Yan-Zhen Zhang, Hui-Ling Li, Li-Ying Sun, Li-Juan Wang, and Ying-Feng Han*



Cite This: *J. Am. Chem. Soc.* 2023, 145, 7446–7453



Read Online

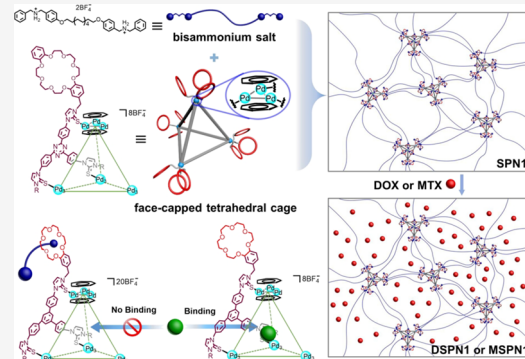
ACCESS |

Metrics & More

Article Recommendations

Supporting Information

ABSTRACT: Herein, a series of face-capped $(Tr_2M_3)_4L_4$ ($Tr = \text{cycloheptatrienyl cationic ring}$; $M = \text{metal}$; $L = \text{organosulfur ligand}$) tetrahedral cages 1–3 functionalized with 12 appended crown ether moieties were designed and synthesized. The reversible binding of ammonium cations with peripheral crown ether moieties to adjust internal guest-binding was realized. Combination of a bisammonium linker and cage 3 led to the formation of a supramolecular gel SPN1 via host–guest interactions between the crown ether moieties and ammonium salts. The obtained supramolecular gel exhibited multiple-stimuli responsiveness, injectability, and excellent self-healing properties and could be further developed to a SPN1-based drug delivery system. In addition, the storage modulus of SPN1 was 20 times higher than that of the model gel without Pd–Pd bonded blocks, and SPN1 had better self-healing properties compared with the latter, demonstrating the importance of such cages in improving mechanical strength without losing the dynamic properties of the material. The cytotoxicity in vitro of the drug-loaded (doxorubicin or methotrexate) SPN1 was significantly improved compared to that of free drugs.



INTRODUCTION

Hierarchical self-assembly (HAS) involving multiple independent interactions has attracted much attention as an effective strategy to construct various complex biological superstructures.¹ Inspired by nature, hierarchical combinations containing orthogonal coordination-driven self-assembly and other noncovalent interactions provide insight into the construction of supramolecular structures and supramolecular polymer networks (SPNs) with higher-order structures and desired functions.^{2–4} Among them, SPNs formed by orthogonal fashion cross-linking coordination cages with well-defined geometries and dimensions can not only improve the mechanical strength of supramolecular gel while maintaining dynamic properties, but also their inherent cavities can enable materials with additional excellent functionalities, such as catalysis, recognition, separation, and fluorescence.^{5–7} The properties of such complex functional materials are highly dependent on coordination cage-centered building blocks. Thus, the introduction of coordination cages with a novel structure may force them to generate new functions and applications.

Utilizing metal clusters, particularly metal–metal bonded clusters, and replacing a single metal ion to trigger coordination-driven self-assembly make the size of internal cavity, structural diversity, and integrity of coordination cages comprehensively improved and can entrust them richer

physicochemical properties as well as broader applications.^{2,8,9} Recently, a library of lipid-soluble and water-soluble face-capped tetrahedral cages with metal–metal bonded coordination blocks that can adaptively and selectively recognize and separate a range of guests have been developed.¹⁰ However, until now, there is still destitute of employing coordination cages with metal–metal bonded nodes as building blocks to construct higher-order architectures beyond the nanoscale in size and in form of soft materials. Toward this end, we envisioned to introduce such cages with metal–metal bonded clusters as the core to construct a novel higher-order system through the HAS strategy.

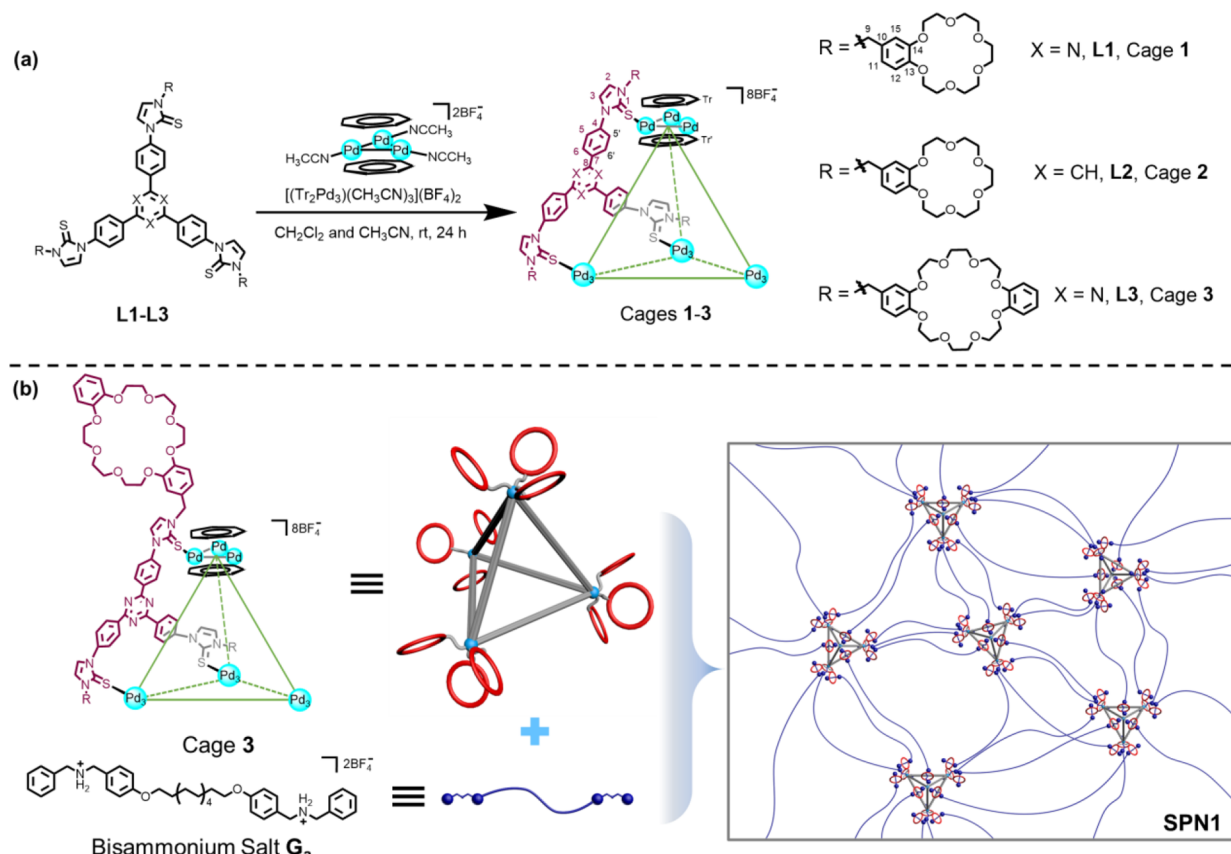
Herein, face-capped tetrahedral cages 1–3 each of which bore 12 crown ether moieties can be prepared by organosulfur ligands L1–L3 and the cycloheptatrienyl tripalladium complex $[Tr_2Pd_3(CH_3CN)_3](BF_4)_2$ ($Tr = \text{cycloheptatrienyl cationic ring}$) (Scheme 1a). The host–guest interaction of 2 was studied, revealing that the internal tetrahedral cavity may be regulated to encapsulate the guest by controlling the external

Received: January 2, 2023

Published: March 22, 2023



Scheme 1. (a) Synthesis of Face-Capped Tetrahedral Cages 1–3 and (b) Formation of Cross-Linked Supramolecular Polymer Network SPN1 from Cage 3 and Bisammonium Salt G_a



crown ether-based multivalent binding effect. Subsequently, orthogonal metal–ligand interaction and host–guest interaction of crown ether have been utilized to integrate 3 on the supramolecular polymeric material for preparing a supramolecular gel SPN1, where the tetrahedral cavities were contained in an extended network (**Scheme 1b**). In addition, the obtained SPN1 also exhibited stimulus responsiveness, injectability, and self-healing ability. Compared with model gel SPN2 without Pd–Pd bonded blocks based on L3, face-capped tetrahedral cage-based gel SPN1 has a higher modulus and better self-healing performance. Furthermore, we also studied the drug delivery of metallogegel SPN1. The results in vitro have shown that the cytotoxicity of doxorubicin (DOX) and methotrexate (MTX) was significantly enhanced via the SPN1-based drug delivery system.

RESULTS AND DISCUSSION

Ligand Design and Synthesis. First, trisimidazolium salts a–c featuring three benzo-18-crown-6 (B18C6) or dibenzo-24-crown-8 (DB24C8) units were prepared according to the reported procedure.¹¹ Trisimidazolium salts a–c reacted with K_2CO_3 and sulfur powder to obtain corresponding ligands L1–L3 appended with three B18C6 or DB24C8 units in 82–88% yield, as depicted in **Scheme S1** (see the Supporting Information, SI). Ligands L1–L3 were fully characterized by 1H , $^{13}C\{^1H\}$ nuclear magnetic resonance (NMR) spectroscopy (see the SI, **Figures S1–S6**). The 1H NMR spectra (in $CDCl_3$) of ligands L1–L3 showed no resonance signals for imidazolium N–CH–N protons which suggested the complete formation of organosulfur linkers.

Construction of Face-Capped Tetrahedral Cages. The reaction of ligands L1–L3 and the cycloheptatrienyl tripalladium complex $[(Tr_2Pd_3)(CH_3CN)_3](BF_4)_2$ in acetonitrile and dichloromethane (1:1) at ambient temperature resulted in face-capped tetrahedral cages 1–3 in which 12 B18C6 or DB24C8 units were appended on the N-wingtips (**Scheme 1a**). Cages 1–3 were obtained in excellent yield of 94–97% and were unambiguously characterized by NMR spectroscopy (1H , $^{13}C\{^1H\}$, and 2D NMR) and high-resolution-electrospray ionization (HR-ESI) mass spectrometry (see the SI, **Figures S7–S26**). Two sharp singlet signals assigned to the cycloheptatrienyl cationic rings were observed in the 1H NMR spectra of cages 1–3. For instance, the formation of a single species represented cage 1 was revealed by diffusion-ordered NMR spectroscopy (DOSY) by exhibiting a single band at a diffusion coefficient of $D = 8.32 \times 10^{-10} m^2 s^{-1}$ ($\log D = -9.08$) (**Figure 1**). Furthermore, the HR-ESI mass spectrum (positive ion mode) of 1 showed the corresponding peak at $m/z = 1199.9459$ (calcd for $[1 - 7BF_4]^{7+}$ 1199.9471) which was in good agreement with its theoretical distribution (**Figure S12**). Unfortunately, all attempts to obtain single crystals of face-capped tetrahedral cages 1–3 bearing 12 crown ethers suitable for X-ray analysis have so far been unsuccessful. However, based on our previous work¹⁰ and the characterization of NMR spectroscopy and HR-ESI mass spectrometry, we surmised that the assemblies 1–3 confirm the structure of the tetrahedral complexes, as depicted in **Scheme 1a**.

Guest-Binding Properties. Reversible multivalent binding effects may serve as an efficient method to tune the encapsulation of guests by the cavity of coordination cages.¹²

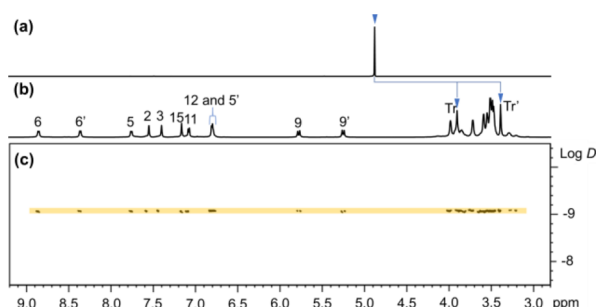


Figure 1. ^1H NMR spectra (CD_3CN , 400 MHz, 298 K) of (a) $[(\text{Tr}_2\text{Pd}_3)(\text{CH}_3\text{CN})_3]_2(\text{BF}_4)_2$ and (b) Cage 1. (c) ^1H DOSY spectrum of cage 1. Cycloheptatrienyl cationic protons were represented by asterisks (blue downward pointing triangle).

Cages 1–3 can encapsulate guests in two ways: using an internal tetrahedral cavity to bind guests or employing external crown ether units to bind cationic guests. We attempted to explore any relationship between two host–guest interactions in this new system (Figure 2). At the beginning, the interaction

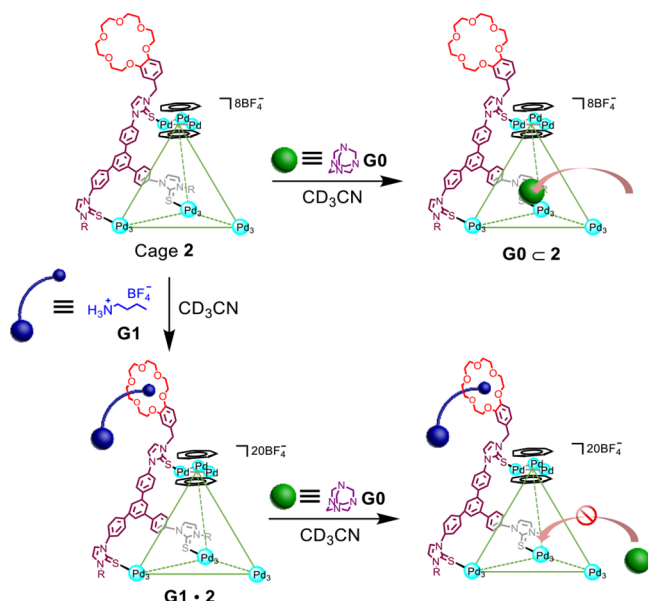


Figure 2. Schematic diagram of inhibiting cage 2 encapsulating guest $\text{G}0$ by controlling crown ether combined with ammonium salt $\text{G}1$.

between the cavity of cage 2 and hexamethylenetetramine ($\text{G}0$) was confirmed when excess $\text{G}0$ (30 equiv) was added to a CD_3CN solution of 2 (Figure S27). In particular, cycloheptatrienyl cationic ring protons $\text{H}_{\text{Tr}'}$ located in the interior of the tetrahedral cavity exhibit an obvious upfield shift to $\delta = 3.28$ ppm ($\Delta\delta = 0.28$ ppm) and protons $\text{H}9$ experienced a downfield shift to $\delta = 8.09$ ppm ($\Delta\delta = 0.06$ ppm), indicating the formation of inclusion complex.¹⁰ ^1H NMR integration indicated $\sim 43\%$ formation of the 1:1 host–guest complex $\text{G}0 \subset 2$.

In contrast, the recognition mode between the external B18C6 units and guests was observed when ammonium salt $\text{G}1$ was added to the solution of cage 2. The formation of host–guest complex $\text{G}1 \cdot 2$ based on the interactions of external crown ether moieties and ammonium salts was unambiguously characterized by NMR spectroscopy (^1H , $^{13}\text{C}\{\text{H}\}$, and 2D NMR) (Figures S28–S32). Characteristic shifts of ^1H NMR in

CD_3CN caused by host–guest complexation of $\text{G}1$ and cage 2 were observed, where methylene protons H_a on $\text{G}1$ experienced significant upfield shifts and protons H_e on $\text{G}1$ experienced obvious downfield shifts (Figure S28). However, no host–guest complex within the internal cavity was formed when excess $\text{G}0$ was added to a CD_3CN solution of the host–guest complex $\text{G}1 \cdot 2$ (Figure S33). After removal of the binding ammonium salts, the formation of $\text{G}0 \subset 2$ can be detected. This may be due to the external larger sterically hindered units restricting the flexibility of the cage or blocking the cage portals to inhibit further encapsulation.^{12,13} These results indicated that the process of encapsulating guests in internal tetrahedral cavities can be controlled by tuning the multivalent binding effect of the peripheral crown ether units.

Formation of a Supramolecular Gel. For SPNs based on coordination cages, it is very important to ensure that metal–ligand interaction and other noncovalent interaction can coexist stably and function independently.¹⁴ As the interaction between cage 3 and the secondary ammonium salt $\text{G}2$ was established, the stable and orthogonal coexistence of metal–ligand interaction and crown ether-based recognition motifs can be confirmed (see the SI, Figures S34–S36). Subsequently, we tried to utilize this multifunctional core as a building block to construct a cage-core supramolecular polymer network SPN1, in which each terminal binding site of bisammonium salt G_a bearing a long alkyl chain spacer was anchored in the cavity of each crown ether (Scheme 1b). An experiment of the host–guest complexation with G_a and 3 was studied (Figure S37). It was obvious that the protons of G_a underwent an obvious chemical shift consistent with slow exchange on the NMR time scale, which meant the occurrence of host–guest interaction.

Moreover, the above-mentioned two-component systems ($3:\text{G}_a = 1:6$) from 2, 6, 10, 14, and 18 mM based on cage 3 have been prepared. According to the concentration-dependent ^1H NMR spectra, the proton signals became wider when the concentration was higher, which indicated the formation of polymeric components with high molecular weight (Figure S38). In order to determine the size of SPN1 in the solution, we performed the concentration-dependent DOSY measurement. As the concentration of 3 in the two-component system increased from 2 to 18 mM, the measured weight average diffusion coefficient (D) decreased from 3.72×10^{-9} to $9.71 \times 10^{-11} \text{ m}^2 \text{ s}^{-1}$ ($D_{2 \text{ mM}}/D_{18 \text{ mM}} = 38.31$) (Figure 3a). Generally, it is recognized that a reduction of the diffusion coefficient by more than 10-fold is confirmed on an important basis for the formation of supramolecular polymer.^{11,15} SEM revealed the surface morphology of the xerogel prepared by freeze-drying

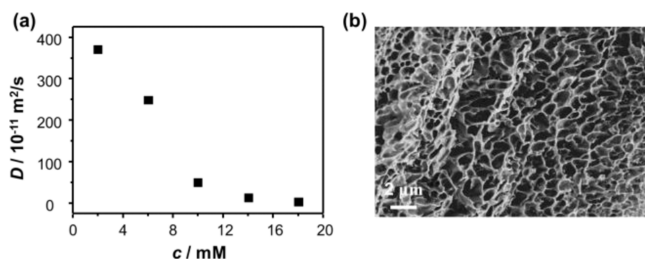


Figure 3. (a) Concentration dependence of diffusion coefficient D (CD_3CN , 600 MHz, 298 K) of SPN1. (b) Scanning electron microscopy (SEM) image of SPN1 formed by a freeze-drying method.

methodology, showing three-dimensional cross-linked porous networks (Figure 3b).

Next the gelation experiment of **SPN1** was carried out (Figure 4a). When the concentration of 3 in two-component

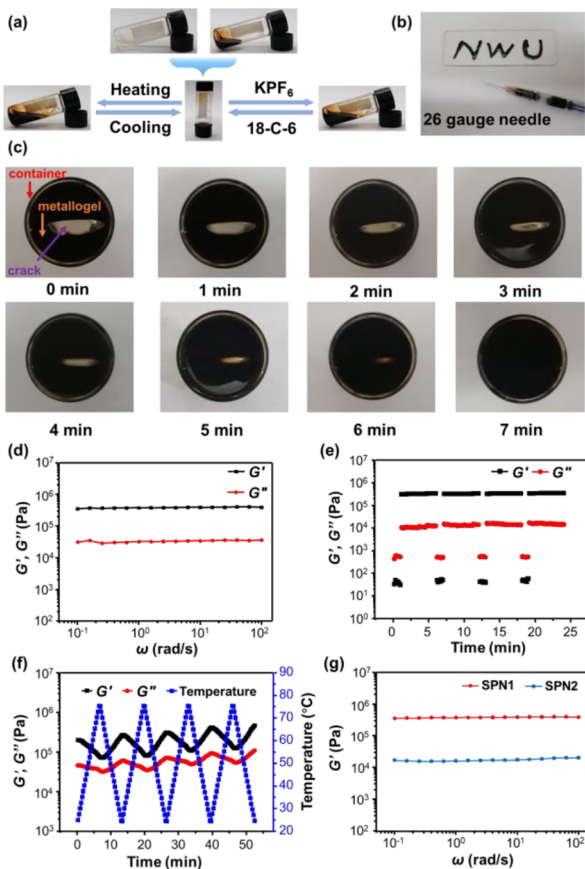


Figure 4. (a) Reversible gel–sol transition of **SPN1**. (b) Injectable behavior of **SPN1**. (c) Self-healing process of **SPN1**. (d) Storage modulus (G') and loss modulus (G'') versus frequency (ω) for **SPN1**. (e) G' and G'' of **SPN1** in continuous step strain measurements that 300% strain for 60 s was applied to **SPN1**, and then the strain was released to 0.1% for 300 s; four cycles were completed. (f) Reversible temperature-dependent rheological tests: G' and G'' of **SPN1**. (g) G' of **SPN1** and **SPN2** versus ω .

acetonitrile solution increased to 30 mM, a coordination cage-core supramolecular gel of **SPN1** can be constructed immediately. Surprisingly, the reversible gel–sol transition can be triggered through the operation of heating and cooling or adding and removing K^+ . Because the host–guest interaction between DB24C8 and ammonium salt weakened after heating over 60 °C, the metalloge **SPN1** collapsed. The metalloge **SPN1** restored when returning to room temperature. After introducing 12 equivalent amounts of KPF₆, host–guest interaction was blocked due to the DB24C8 units forming a 1:1 complex with K^+ , inducing the disassembly of the metalloge. The interaction of DB24C8 units and G_a can be restored by introducing excess 18-crown-6 (18C6) to combine K^+ , leading to the recovery of the metalloge. We used rhodamine as a trace dye to verify the ion response capability of **SPN1** that neutral and acidic phosphate buffered saline (PBS) cannot cause the dissociation of **SPN1** including rhodamine salts, and **SPN1** released relatively more rhodamine due to the presence of potassium ions (Figures S39 and S40).

Injectable ability of the metalloge **SPN1** was observed by squeezing it smoothly and evenly with the help of a 26-gauge needle syringe (Figure 4b). As shown in Figure 4c, when the metalloge **SPN1** broken for 7 minutes, the crack on the gel can be repaired completely, reflecting visible self-healing properties. As the metalloge **SPN1** was destroyed by external force, the noncovalent interaction that accompanied the wound position was also dissociated accordingly. However, the dynamic and reversible recognition procedures effectively controlled the self-healing process, causing the metalloge **SPN1** to trigger healing in a short time.

Rheological Experiments. In order to further characterize the obtained metalloge **SPN1**, we also performed rheological experiments. Strain sweep results of the metalloge **SPN1** showed that the linear response (the storage modulus $G' >$ the loss modulus G'') was reflected before the critical strain zone ($\gamma = 2\%$). G' and G'' values dropped rapidly when the applied strain increased further, while $G' < G''$ as **SPN1** was imposed the strain over 100%, that can be ascribed to the disassembly of **SPN1** (Figure S41). In addition, the frequency sweep tests reflected that the G' value remained and G' was larger than G'' over a wide range of frequencies, which represented the quasi-solid property of the metalloge **SPN1** (Figure 4d). The viscosity of **SPN1** decreased with the frequency increase (Figure S42). Subsequently, the metalloge **SPN1** suffers large (300%) and little (0.1%) strains, respectively (Figure 4e). When **SPN1** was kept for 60 s under 300% strain, G' was below G'' , suggesting that the metalloge **SPN1** was broken. Next both G' and G'' restored to their original values when the strain was reverted to 0.1%. There was not any loss of modulus among the repeated process for four cycles, indicating excellent self-healing properties of the metalloge **SPN1**. Reversible temperature-dependent rheological tests of the metalloge **SPN1** were also carried out (Figure 4f) and showed that temperature-dependent behavior over the test always revealed $G' > G''$ in the four sets of temperature-dependent cycling. Moreover, G' and G'' decreased with increasing temperature and increased roughly to the original modulus with decreasing temperature, representing dissociation and recovery of the metalloge **SPN1** respectively. The results confirmed the reversible behavior of the metalloge **SPN1** to temperature-dependent cycling.

Supramolecular gels were dedicated to trying to convert molecular-level information into material properties through one or more noncovalent interactions.¹⁶ Thus, it is necessary to explore any influence of such a cage with metal–metal bonded units on the supramolecular gel. We also prepared a model gel of **SPN2** based on ligand **L3** and **G_a** through a similar self-assembly procedure of forming **SPN1** as a comparison (Figure S43). The critical gelation concentration of the gel **SPN2** was determined to be 180 mM based on **L3** blocks. Rheological experiments of the model gel **SPN2** were carried out to further compare the performance of the two gels whose concentration (based on the DB24C8/ammonium salt units) remained consistent (Figures S44 and S45). Similarly, the frequency sweep tests showed that G' was larger than G'' and G' was independent of frequency ω , indicating the construction of **SPN2** (Figure S45). However, it was obvious that **SPN2** was not as stiff as **SPN1**, because G' of **SPN1** was ca. 20-fold that of **SPN2** (Figure 4g). We attributed the phenomenon to higher branch properties provided by multipoint interaction and the rigidity of cages based on Pd–Pd bonded units.^{5,17,18} Subsequently, the model gel **SPN2**

was studied under large (300%) and small (0.1%) strains, and G' only recovered to 58% of the original value after four cycles, indicating that the self-healing performance of the gel **SPN1** was significantly weaker than that of the metallogele **SPN1** (**Figure S46**). These results demonstrated the truth that the existence of cage **3** can effectively improve stiffness and self-healing properties of the material.

Drug Delivery System. Encouraged by the excellent performance with respect to both K^+ -responsive and optimally adaptive functions, we then studied the cytocompatibility and drug delivery of **SPN1** *in vitro*. The **SPN1**-based drug delivery system was designed in **Figure 5a**. MDA-MB-231 human breast

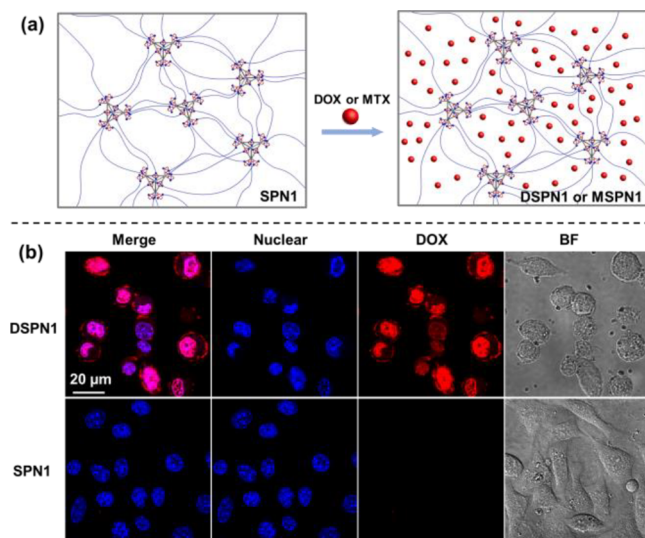


Figure 5. (a) Cartoon representation of the formation of **DSPN1** and **MSPN1**. (b) Confocal laser scanning microscopy (CLSM) images of MDA-MB-231 cells incubated with **DSPN1** and **SPN1**.

cancer cell line and mouse fibroblast cell L929 were selected for testing cell cytotoxicity of **SPN1** and later drug delivery system. From the results displayed in **Figure S47**, the cell viability of drug-free **SPN1** groups was 74.69% in L929 cells and 93.86% in MDA-MB-231 cells even at 100 $\mu\text{g}/\text{mL}$ **SPN1**, respectively. It suggested that **SPN1** has great potential as an efficient drug delivery vehicle due to its excellent cytocompatibility. Subsequently, free drugs were incubated with xerogel **SPN1** to obtain **SPN1** loaded with DOX (**DSPN1**) or MTX (**MSPN1**), which may be due to the combination caused by noncovalent interaction (**Figures S48 and S49**).¹⁹ Cell cytotoxicity of **DSPN1** or **MSPN1** against MDA-MB-231 cell at various concentrations was then evaluated (**Figure S50**). The toxicity against MDA-MB-231 cells increased significantly by **DSPN1** and **MSPN1** drug delivery systems. Most notably, the IC_{50} value of **DSPN1** (0.20 $\mu\text{g}/\text{mL}$) was two orders of magnitude less than that of free DOX (44.55 $\mu\text{g}/\text{mL}$), as shown in **Table S1**. The enhanced cytotoxicity might be attributed to the improved intracellular uptake and intracellular constant drug release.²⁰ These results indicated that **SPN1** with excellent cytocompatibility can be used as an efficient drug delivery vehicle.

The intracellular drug release was also observed by CLSM. As shown in **Figure 5b**, DOX (red fluorescence) mostly colocalizes with the nuclei (blue fluorescence), demonstrating that **DSPN1** could effectively deliver DOX into nuclei of cancer cells and thereby significantly enhance the efficacy of

chemotherapy. The above results have demonstrated that **DSPN1** were taken up by cells and can effectively deliver their drug load to MDA-MB-231 cell nuclei, resulting in high cytotoxicity in breast cancer cell lines.

CONCLUSIONS

In conclusion, we developed a series of face-capped tetrahedral cages **1–3** incorporating triangular metal–metal-bonded coordination vertices, functionalized with appended crown ethers at N-wingtips. The process of encapsulating guest into the inner cavity of cage **2** can be suppressed by the multivalent binding effect of external crown ethers. In addition, a multifunctional supramolecular gel **SPN1** from cage **3** with triangular metal–metal bonded units was also constructed, through the orthogonal metal–ligand interaction and host–guest interaction. The metallogele **SPN1** exhibited multiple-stimuli responsiveness, injectability, and self-healing properties. More importantly, stiffness and self-healing properties of the material can be significantly improved while retaining its dynamic properties via the intervention of such cages. Further study suggested that biocompatible **SPN1** may serve as an effective stimulus-responsive vehicle for drug delivery system, due to dynamic and tunable noncovalent interactions. We believe that this work has great reference significance for the preparation and application of high-dimensional supramolecular structures and polymeric materials based on coordination cages with metal–metal bonded units through the HAS strategy.

ASSOCIATED CONTENT

Supporting Information

The Supporting Information is available free of charge at <https://pubs.acs.org/doi/10.1021/jacs.3c00024>.

Experimental details for all new compounds with synthesis, characterization, spectra (^1H NMR, $^{13}\text{C}\{^1\text{H}\}$ NMR, and multinuclear NMR spectra, ESI-MS spectra), rheological data, and anticancer study ([PDF](#))

AUTHOR INFORMATION

Corresponding Author

Ying-Feng Han — Key Laboratory of Synthetic and Natural Functional Molecule Chemistry of the Ministry of Education, Xi'an Key Laboratory of Functional Supramolecular Structure and Materials, College of Chemistry and Materials Science, Northwest University, Xi'an 710127, P. R. China; [orcid.org/0000-0002-9829-4670](#); Email: yfhan@nwu.edu.cn

Authors

Zi-En Zhang — Key Laboratory of Synthetic and Natural Functional Molecule Chemistry of the Ministry of Education, Xi'an Key Laboratory of Functional Supramolecular Structure and Materials, College of Chemistry and Materials Science, Northwest University, Xi'an 710127, P. R. China

Yi-Fan Zhang — Key Laboratory of Synthetic and Natural Functional Molecule Chemistry of the Ministry of Education, Xi'an Key Laboratory of Functional Supramolecular Structure and Materials, College of Chemistry and Materials Science, Northwest University, Xi'an 710127, P. R. China

Yan-Zhen Zhang — Key Laboratory of Synthetic and Natural Functional Molecule Chemistry of the Ministry of Education, Xi'an Key Laboratory of Functional Supramolecular

Structure and Materials, College of Chemistry and Materials Science, Northwest University, Xi'an 710127, P. R. China

Hui-Ling Li – Key Laboratory of Synthetic and Natural Functional Molecule Chemistry of the Ministry of Education, Xi'an Key Laboratory of Functional Supramolecular Structure and Materials, College of Chemistry and Materials Science, Northwest University, Xi'an 710127, P. R. China

Li-Ying Sun – Key Laboratory of Synthetic and Natural Functional Molecule Chemistry of the Ministry of Education, Xi'an Key Laboratory of Functional Supramolecular Structure and Materials, College of Chemistry and Materials Science, Northwest University, Xi'an 710127, P. R. China

Li-Juan Wang – Key Laboratory of Synthetic and Natural Functional Molecule Chemistry of the Ministry of Education, Xi'an Key Laboratory of Functional Supramolecular Structure and Materials, College of Chemistry and Materials Science, Northwest University, Xi'an 710127, P. R. China

Complete contact information is available at:

<https://pubs.acs.org/10.1021/jacs.3c00024>

Author Contributions

All authors have given approval to the final version of the manuscript.

Notes

The authors declare no competing financial interest.

ACKNOWLEDGMENTS

This work was supported by the National Natural Science Foundation of China (22025107), the National Youth Top-notch Talent Support Program of China, the Key Science and Technology Innovation Team of Shaanxi Province (2019TD-007), Xi'an Key Laboratory of Functional Supramolecular Structure and Materials, and the FM&EM International Joint Laboratory of Northwest University.

REFERENCES

- (1) (a) Keizer, H. M.; Sijbesma, R. P. Hierarchical Self-Assembly of Columnar Aggregates. *Chem. Soc. Rev.* **2005**, *34*, 226–234. (b) Cheng, C.; Li, S.; Thomas, A.; Kotov, N. A.; Haag, R. Functional Graphene Nanomaterials Based Architectures: Biointeractions, Fabrications, and Emerging Biological Applications. *Chem. Rev.* **2017**, *117*, 1826–1914. (c) Yang, S.; Jiang, L. Biomimetic Self-Assembly of Subcellular Structures. *Chem. Commun.* **2020**, *56*, 8342–8354. (d) Li, F.; Clegg, J. K.; Goux-Capes, L.; Chastanet, G.; D'Alessandro, D. M.; Létard, J.-F.; Kepten, C. J. A Mixed-Spin Molecular Square with a Hybrid [2×2] Grid/Metallocyclic Architecture. *Angew. Chem., Int. Ed.* **2011**, *50*, 2820–2823.
- (2) (a) Roberts, D. A.; Pilgrim, B. S.; Nitschke, J. R. Covalent Post-Assembly Modification in Metallosupramolecular Chemistry. *Chem. Soc. Rev.* **2018**, *47*, 626–644. (b) Li, Y.; Yu, J.-G.; Ma, L.-L.; Li, M.; An, Y.-Y.; Han, Y.-F. Strategies for the Construction of Supramolecular Assemblies from Poly-NHC Ligand Precursors. *Sci. China: Chem.* **2021**, *64*, 701–718. (c) Chen, L.-J.; Yang, H.-B.; Shionoya, M. Chiral Metallosupramolecular Architectures. *Chem. Soc. Rev.* **2017**, *46*, 2555–2576. (d) Cook, T. R.; Stang, P. J. Recent Developments in the Preparation and Chemistry of Metallacycles and Metallacages via Coordination. *Chem. Rev.* **2015**, *115*, 7001–7045. (e) McConnell, A. J.; Wood, C. S.; Neelakandan, P. P.; Nitschke, J. R. Stimuli-Responsive Metal–Ligand Assemblies. *Chem. Rev.* **2015**, *115*, 7729–7793. (f) Lu, Y.; Zhang, H.-N.; Jin, G.-X. Molecular Borromean Rings Based on Half-Sandwich Organometallic Rectangles. *Acc. Chem. Res.* **2018**, *51*, 2148–2158. (g) Li, X.-Z.; Tian, C.-B.; Sun, Q.-F. Coordination-Directed Self-Assembly of Functional Polynuclear Lanthanide Supramolecular Architectures. *Chem. Rev.* **2022**, *122*, 6374–6458. (h) Wu, K.; Li, K.; Chen, S.; Hou, Y.-J.; Lu, Y.-L.; Wang, J.-S.; Wei, M.-J.; Pan, M.; Su, C.-Y. The Redox Coupling Effect in a Photocatalytic Ru^{II}-Pd^{II} Cage with TTF Guest as Electron Relay Mediator for Visible-Light Hydrogen-Evolving Promotion. *Angew. Chem., Int. Ed.* **2020**, *59*, 2639–2643. (i) Wang, H.; Wang, K.; Xu, Y.; Wang, W.; Chen, S.; Hart, M.; Wojtas, L.; Zhou, L.-P.; Gan, L.; Yan, X.; Li, Y.; Lee, J.; Ke, X.-S.; Wang, X.-Q.; Zhang, C.-W.; Zhou, S.; Zhai, T.; Yang, H.-B.; Wang, M.; He, J.; Sun, Q.-F.; Xu, B.; Jiao, Y.; Stang, P. J.; Sessler, J. L.; Li, X. Hierarchical Self-Assembly of Nanowires on the Surface by Metallo-Supramolecular Truncated Cuboctahedra. *J. Am. Chem. Soc.* **2021**, *143*, 5826–5835. (j) Yang, D.; Zhao, J.; Zhao, Y.; Lei, Y.; Cao, L.; Yang, X.-J.; Davi, M.; de Sousa Amadeu, N.; Janiak, C.; Zhang, Z.; Wang, Y.-Y.; Wu, B. Encapsulation of Halocarbons in a Tetrahedral Anion Cage. *Angew. Chem., Int. Ed.* **2015**, *54*, 8658–8661. (k) Saha, R.; Mondal, B.; Mukherjee, P. S. Molecular Cavity for Catalysis and Formation of Metal Nanoparticles for Use in Catalysis. *Chem. Rev.* **2022**, *122*, 12244–12307. (l) Klosterman, J. K.; Yamauchi, Y.; Fujita, M. Engineering Discrete Stacks of Aromatic Molecules. *Chem. Soc. Rev.* **2009**, *38*, 1714–1725. (m) Lee, H.; Tessarolo, J.; Langbehn, D.; Baksi, A.; Herges, R.; Clever, G. H. Light-Powered Dissipative Assembly of Diazocine Coordination Cages. *J. Am. Chem. Soc.* **2022**, *144*, 3099–3105. (n) Wu, K.; Tessarolo, J.; Baksi, A.; Clever, G. H. Guest-Modulated Circularly Polarized Luminescence by Ligand-to-Ligand Chirality Transfer in Heteroleptic Pd^{II} Coordination Cages. *Angew. Chem., Int. Ed.* **2022**, *61*, No. e202205725.
- (3) (a) Chen, L.-J.; Yang, H.-B. Construction of Stimuli-Responsive Functional Materials via Hierarchical Self-Assembly Involving Coordination Interactions. *Acc. Chem. Res.* **2018**, *51*, 2699–2710. (b) Li, B.; He, T.; Fan, Y.; Yuan, X.; Qiu, H.; Yin, S. Recent Developments in the Construction of Metallacycle/Metallacage-Cored Supramolecular Polymers via Hierarchical Self-Assembly. *Chem. Commun.* **2019**, *55*, 8036–8059. (c) Sun, Y.; Chen, C.; Stang, P. J. Soft Materials with Diverse Suprastructures via the Self-Assembly of Metal–Organic Complexes. *Acc. Chem. Res.* **2019**, *52*, 802–817. (d) Datta, S.; Saha, M. L.; Stang, P. J. Hierarchical Assemblies of Supramolecular Coordination Complexes. *Acc. Chem. Res.* **2018**, *51*, 2047–2063. (e) Zhang, W.; Yang, D.; Zhao, J.; Hou, L.; Sessler, J. L.; Yang, X.-J.; Wu, B. Controlling the Recognition and Reactivity of Alkyl Ammonium Guests Using an Anion Coordination-Based Tetrahedral Cage. *J. Am. Chem. Soc.* **2018**, *140*, 5248–5256.
- (4) (a) Xia, D.; Wang, P.; Ji, X.; Khashab, N. M.; Sessler, J. L.; Huang, F. Functional Supramolecular Polymeric Networks: The Marriage of Covalent Polymers and Macrocycle-Based Host–Guest Interactions. *Chem. Rev.* **2020**, *120*, 6070–6123. (b) Lu, W.; Le, X.; Zhang, J.; Huang, Y.; Chen, T. Supramolecular Shape Memory Hydrogels: A New Bridge Between Stimuli-Responsive Polymers and Supramolecular Chemistry. *Chem. Soc. Rev.* **2017**, *46*, 1284–1294. (c) Löwenberg, C.; Balk, M.; Wischke, C.; Behl, M.; Lendlein, A. Shape-Memory Hydrogels: Evolution of Structural Principles to Enable Shape Switching of Hydrophilic Polymer Networks. *Acc. Chem. Res.* **2017**, *50*, 723–732. (d) Webber, M. J.; Langer, R. Drug Delivery by Supramolecular Design. *Chem. Soc. Rev.* **2017**, *46*, 6600–6620. (e) Huang, G.; Li, F.; Zhao, X.; Ma, Y.; Li, Y.; Lin, M.; Jin, G.; Lu, T. J.; Genin, G. M.; Xu, F. Functional and Biomimetic Materials for Engineering of the Three-Dimensional Cell Microenvironment. *Chem. Rev.* **2017**, *117*, 12764–12850. (f) Yan, X.; Liu, Z.; Zhang, Q.; Lopez, J.; Wang, H.; Wu, H.-C.; Niu, S.; Yan, H.; Wang, S.; Lei, T.; Li, J.; Qi, D.; Huang, P.; Huang, J.; Zhang, Y.; Wang, Y.; Li, G.; Tok, J. B.-H.; Chen, X.; Bao, Z. Quadruple H-Bonding Cross-Linked Supramolecular Polymeric Materials as Substrates for Stretchable, Antitearing, and Self-Healable Thin Film Electrodes. *J. Am. Chem. Soc.* **2018**, *140*, 5280–5289. (g) Zhao, D.; Zhang, Z.; Zhao, J.; Liu, K.; Liu, Y.; Li, G.; Zhang, X.; Bai, R.; Yang, X.; Yan, X. A Mortise-and-Tenon Joint Inspired Mechanically Interlocked Network. *Angew. Chem., Int. Ed.* **2021**, *60*, 16224–16229. (h) Zhang, Z.; Cheng, L.; Zhao, J.; Wang, L.; Liu, K.; Yu, W.; Yan, X. Synergistic Covalent and Supramolecular Polymers for Mechanically Robust but Dynamic Materials. *Angew. Chem., Int. Ed.* **2020**, *59*, 12139–12146. (i) Purba, P. C.; Maity, M.; Bhattacharyya, S.; Mukherjee, P. S. A Self-Assembled

- Palladium(II) Barrel for Binding of Fullerenes and Photosensitization Ability of the Fullerene-Encapsulated Barrel. *Angew. Chem., Int. Ed.* **2021**, *60*, 14109–14116. (j) Hong, C. M.; Bergman, R. G.; Raymond, K. N.; Toste, F. D. Self-Assembled Tetrahedral Hosts as Supramolecular Catalysts. *Acc. Chem. Res.* **2018**, *51*, 2447–2455. (k) Brown, C. J.; Toste, F. D.; Bergman, R. G.; Raymond, K. N. Supramolecular Catalysis in Metal–Ligand Cluster Hosts. *Chem. Rev.* **2015**, *115*, 3012–3035. (l) Miyamura, H.; Bergman, R. G.; Raymond, K. N.; Toste, F. D. Heterogeneous Supramolecular Catalysis through Immobilization of Anionic M_4L_6 Assemblies on Cationic Polymers. *J. Am. Chem. Soc.* **2020**, *142*, 19327–19338. (m) Tessarolo, J.; Lee, H.; Sakuda, E.; Umakoshi, K.; Clever, G. H. Integrative Assembly of Heteroleptic Tetrahedra Controlled by Backbone Steric Bulk. *J. Am. Chem. Soc.* **2021**, *143*, 6339–6344.
- (5) (a) Liu, J.; Wang, Z.; Cheng, P.; Zaworotko, M. J.; Chen, Y.; Zhang, Z. Post-Synthetic Modifications of Metal–Organic Cages. *Nat. Rev. Chem.* **2022**, *6*, 339–356. (b) Chen, L.; Chen, Q.; Wu, M.; Jiang, F.; Hong, M. Controllable Coordination-Driven Self-Assembly: From Discrete Metallocages to Infinite Cage-Based Frameworks. *Acc. Chem. Res.* **2015**, *48*, 201–210. (c) Jahović, I.; Zou, Y.-Q.; Adorinni, S.; Nitschke, J. R.; Marchesan, S. Cages Meet Gels: Smart Materials with Dual Porosity. *Matter* **2021**, *4*, 2123–2140. (d) Zhang, D.; Ronson, T. K.; Zou, Y.-Q.; Nitschke, J. R. Metal–Organic Cages for Molecular Separations. *Nat. Rev. Chem.* **2021**, *5*, 168–182. (e) Mollick, S.; Fajal, S.; Mukherjee, S.; Ghosh, S. K. Stabilizing Metal–Organic Polyhedra (MOP): Issues and Strategies. *Chem. – Asian J.* **2019**, *14*, 3096–3108. (f) Pullen, S.; Tessarolo, J.; Clever, G. H. Increasing Structural and Functional Complexity in Self-Assembled Coordination Cages. *Chem. Sci.* **2021**, *12*, 7269–7293. (g) Gu, Y.; Zhao, J.; Johnson, J. A. Polymer Networks: From Plastics and Gels to Porous Frameworks. *Angew. Chem., Int. Ed.* **2020**, *59*, 5022–5049. (h) Hu, S.-J.; Guo, X.-Q.; Zhou, L.-P.; Yan, D.-N.; Cheng, P.-M.; Cai, L.-X.; Li, X.-Z.; Sun, Q.-F. Guest-Driven Self-Assembly and Chiral Induction of Photo-functional Lanthanide Tetrahedral Cages. *J. Am. Chem. Soc.* **2022**, *144*, 4244–4253.
- (6) (a) Lu, C.; Zhang, M.; Tang, D.; Yan, X.; Zhang, Z.-Y.; Zhou, Z.; Song, B.; Wang, H.; Li, X.; Yin, S.; Sepehrpour, H.; Stang, P. J. Fluorescent Metallacage-Core Supramolecular Polymer Gel Formed by Orthogonal Metal Coordination and Host–Guest Interactions. *J. Am. Chem. Soc.* **2018**, *140*, 7674–7680. (b) Hosono, N.; Kitagawa, S. Modular Design of Porous Soft Materials via Self-Organization of Metal–Organic Cages. *Acc. Chem. Res.* **2018**, *51*, 2437–2446. (c) Sutar, P.; Suresh, V. M.; Jayaramulu, K.; Hazra, A.; Maji, T. K. Binder Driven Self-Assembly of Metal–Organic Cubes towards Functional Hydrogels. *Nat. Commun.* **2018**, *9*, 3587. (d) Zhao, J.; Cheng, L.; Liu, K.; Zhang, Z.; Yu, W.; Yan, X. Metal–Organic Polyhedra Crosslinked Supramolecular Polymeric Elastomers. *Chem. Commun.* **2020**, *56*, 8031–8034. (e) Brown, C. M.; Lundberg, D. J.; Lamb, J. R.; Kevlishvili, I.; Kleinschmidt, D.; Alfaraj, Y. S.; Kulik, H. J.; Ottaviani, M. F.; Oldenhuis, N. J.; Johnson, J. A. Endohedrally Functionalized Metal–Organic Cage-Cross-Linked Polymer Gels as Modular Heterogeneous Catalysts. *J. Am. Chem. Soc.* **2022**, *144*, 13276–13284. (f) Wang, Y.; Zhong, M.; Park, J. V.; Zhukhovitskiy, A. V.; Shi, W.; Johnson, J. A. Block Co-PolyMOCs by Stepwise Self-Assembly. *J. Am. Chem. Soc.* **2016**, *138*, 10708–10715. (g) Liu, J.; Li, J.; Qiao, S.; Wang, Z.; Zhang, P.; Fan, X.; Cheng, P.; Li, Y.-S.; Chen, Y.; Zhang, Z. Self-Healing and Shape Memory Hypercrosslinked Metal–Organic Polyhedra Polymers via Coordination Post-Assembly. *Angew. Chem., Int. Ed.* **2022**, *61*, No. e202212253. (h) Verma, P.; Rahimi, F. A.; Samanta, D.; Kundu, A.; Dasgupta, J.; Maji, T. K. Visible-Light-Driven Photocatalytic CO_2 Reduction to CO/CH_4 Using a Metal–Organic “Soft” Coordination Polymer Gel. *Angew. Chem., Int. Ed.* **2022**, *61*, No. e202116094.
- (7) (a) Wang, L.; Cheng, L.; Li, G.; Liu, K.; Zhang, Z.; Li, P.; Dong, S.; Yu, W.; Huang, F.; Yan, X. A Self-Cross-Linking Supramolecular Polymer Network Enabled by Crown-Ether-Based Molecular Recognition. *J. Am. Chem. Soc.* **2020**, *142*, 2051–2058. (b) Gao, K.; Feng, Q.; Zhang, Z.; Zhang, R.; Hou, Y.; Mu, C.; Li, X.; Zhang, M. Emissive Metallacage-Cored Polyurethanes with Self-Healing and Shape Memory Properties. *Angew. Chem., Int. Ed.* **2022**, *61*, No. e202209958. (c) Jeyakkumar, P.; Liang, Y.; Guo, M.; Lu, S.; Xu, D.; Li, X.; Guo, B.; He, G.; Chu, D.; Zhang, M. Emissive Metallacycle-Crosslinked Supramolecular Networks with Tunable Crosslinking Densities for Bacterial Imaging and Killing. *Angew. Chem., Int. Ed.* **2020**, *59*, 15199–15203. (d) Carné-Sánchez, A.; Craig, G. A.; Larpent, P.; Hirose, T.; Higuchi, M.; Kitagawa, S.; Matsuda, K.; Urayama, K.; Furukawa, S. Self-Assembly of Metal–Organic Polyhedra into Supramolecular Polymers with Intrinsic Micro-porosity. *Nat. Commun.* **2018**, *9*, 2506. (e) Chai, H.; Chen, Z.; Wang, S.-H.; Quan, M.; Yang, L.-P.; Ke, H.; Jiang, W. Enantioselective Recognition of Neutral Molecules in Water by a Pair of Chiral Biomimetic Macrocyclic Receptors. *CCS Chem.* **2020**, *2*, 440–452. (f) Chen, Y.; Wu, G.; Chen, B.; Qu, H.; Jiao, T.; Li, Y.; Ge, C.; Zhang, C.; Liang, L.; Zeng, X.; Cao, X.; Wang, Q.; Li, H. Self-Assembly of a Purely Covalent Cage with Homochirality by Imine Formation in Water. *Angew. Chem., Int. Ed.* **2021**, *60*, 18815–18820.
- (8) (a) Zhu, Z.-Z.; Tian, C.-B.; Sun, Q.-F. Coordination-Assembled Molecular Cages with Metal Cluster Nodes. *Chem. Rec.* **2021**, *21*, 498–522. (b) Huang, R.-W.; Wei, Y.-S.; Dong, X.-Y.; Wu, X.-H.; Du, C.-X.; Zang, S.-Q.; Mak, T. C.-W. Hypersensitive Dual-Function Luminescence Switching of a Silver-Chalcogenolate Cluster-Based Metal–Organic Framework. *Nat. Chem.* **2017**, *9*, 689–697. (c) Tanaka, S.; Tsurugi, H.; Mashima, K. Supramolecular Assemblies of Multi-Nuclear Transition Metal Complexes: Synthesis and Redox Properties. *Coord. Chem. Rev.* **2014**, *265*, 38–51. (d) Yan, L.-L.; Yao, L.-Y.; Ng, M.; Yam, V. W.-W. Stimuli-Responsive and Structure-Adaptive Three-Dimensional Gold(I) Cluster Cages Constructed via “De-aurophilic” Interaction Strategy. *J. Am. Chem. Soc.* **2021**, *143*, 19008–19017. (e) Yan, L.-L.; Yao, L.-Y.; Yam, V. W.-W. Concentration- and Solvation-Induced Reversible Structural Transformation and Assembly of Polynuclear Gold(I) Sulfido Complexes. *J. Am. Chem. Soc.* **2020**, *142*, 11560–11568.
- (9) (a) Zheng, X.-Y.; Kong, X.-J.; Zheng, Z.; Long, L.-S.; Zheng, L.-S. High-Nuclearity Lanthanide-Containing Clusters as Potential Molecular Magnetic Coolers. *Acc. Chem. Res.* **2018**, *51*, 517–525. (b) Ma, L.-L.; Li, Y.; Li, X.; Zhang, L.; Sun, L.-Y.; Han, Y.-F. A Molecular “A-Type” Tangled Metallocube. *Angew. Chem., Int. Ed.* **2022**, *61*, No. e202208376. (c) Tan, C.; Jiao, J.; Li, Z.; Liu, Y.; Han, X.; Cui, Y. Design and Assembly of a Chiral Metallosalen-Based Octahedral Coordination Cage for Supramolecular Asymmetric Catalysis. *Angew. Chem., Int. Ed.* **2018**, *57*, 2085–2090. (d) Guo, T.-T.; Su, X.-F.; Xu, X.; Yang, J.; Yan, L.-K.; Ma, J.-F. A Calix[4]resorcinarene-Based $[Co_{12}]$ Coordination Cage for Highly Efficient Cycloaddition of CO_2 to Epoxides. *Inorg. Chem.* **2019**, *58*, 16518–16523.
- (10) (a) Wang, L.-J.; Li, X.; Bai, S.; Wang, Y.-Y.; Han, Y.-F. Self-Assembly, Structural Transformation, and Guest-Binding Properties of Supramolecular Assemblies with Triangular Metal–Metal Bonded Units. *J. Am. Chem. Soc.* **2020**, *142*, 2524–2531. (b) Wang, L.-J.; Bai, S.; Han, Y.-F. Water-Soluble Self-Assembled Cage with Triangular Metal–Metal-Bonded Units Enabling the Sequential Selective Separation of Alkanes and Isomeric Molecules. *J. Am. Chem. Soc.* **2022**, *144*, 16191–16198.
- (11) Zhang, Z.-E.; An, Y.-Y.; Zheng, B.; Chang, J.-P.; Han, Y.-F. Hierarchical Self-Assembly of Crown Ether Based Metal–Carbene Cages into Multiple Stimuli-Responsive Cross-Linked Supramolecular Metallogel. *Sci. China: Chem.* **2021**, *64*, 1177–1183.
- (12) (a) von Krbek, L. K. S.; Roberts, D. A.; Pilgrim, B. S.; Schalley, C. A.; Nitschke, J. R. Multivalent Crown Ether Receptors Enable Allosteric Regulation of Anion Exchange in an Fe_4L_6 Tetrahedron. *Angew. Chem., Int. Ed.* **2018**, *57*, 14121–14124. (b) Kovbasyuk, L.; Krämer, R. Allosteric Supramolecular Receptors and Catalysts. *Chem. Rev.* **2004**, *104*, 3161–3188. (c) Lister, F. G. A.; Le Bailly, B. A. F.; Webb, S. J.; Clayden, J. Ligand-Modulated Conformational Switching in a Fully Synthetic Membrane-Bound Receptor. *Nat. Chem.* **2017**, *9*, 420–425. (d) Li, Y.; Dong, J.; Gong, W.; Tang, X.; Liu, Y.; Cui, Y.; Liu, Y. Artificial Biomolecular Channels: Enantioselective Transmembrane Transport of Amino Acids Mediated by Homochiral

- Zirconium Metal–Organic Cages. *J. Am. Chem. Soc.* **2021**, *143*, 20939–20951.
- (13) (a) Davis, A. V.; Raymond, K. N. The Big Squeeze: Guest Exchange in an M_4L_6 Supramolecular Host. *J. Am. Chem. Soc.* **2005**, *127*, 7912–7919. (b) Mendez-Arroyo, J.; d’Aquino, A. I.; Chinen, A. B.; Manraj, Y. D.; Mirkin, C. A. Reversible and Selective Encapsulation of Dextromethorphan and β -Estradiol Using an Asymmetric Molecular Capsule Assembled via the Weak-Link Approach. *J. Am. Chem. Soc.* **2017**, *139*, 1368–1371. (c) Setaka, W.; Koyama, A.; Yamaguchi, K. Cage Size Effects on the Rotation of Molecular Gyrotops with 1,4-Naphthalenediyl Rotor in Solution. *Org. Lett.* **2013**, *15*, 5092–5095. (d) Swartjes, A.; White, P. B.; Lammertink, M.; Elemans, J. A. A. W.; Nolte, R. J. M. Host–Guest Exchange of Viologen Guests in Porphyrin Cage Compounds as Studied by Selective Exchange Spectroscopy (1D EXSY) NMR. *Angew. Chem., Int. Ed.* **2021**, *60*, 1254–1262. (e) Maehara, T.; Sekiya, R.; Harada, K.; Haino, T. Tunable Enforced Cavities inside Self-Assembled Capsules. *Org. Chem. Front.* **2019**, *6*, 1561–1566.
- (14) (a) Sun, Y.; Chen, C.; Liu, J.; Stang, P. J. Recent Developments in the Construction and Applications of Platinum-Based Metallacycles and Metallacages via Coordination. *Chem. Soc. Rev.* **2020**, *49*, 3889–3919. (b) Lu, Y.; Lin, J.; Wang, L.; Zhang, L.; Cai, C. Self-Assembly of Copolymer Micelles: Higher-Level Assembly for Constructing Hierarchical Structure. *Chem. Rev.* **2020**, *120*, 4111–4140. (c) Cao, A.; Hu, J.; Wan, L. Morphology Control and Shape Evolution in 3D Hierarchical Superstructures. *Sci. China: Chem.* **2012**, *55*, 2249–2256.
- (15) (a) Wang, X.-Q.; Wang, W.; Yin, G.-Q.; Wang, Y.-X.; Zhang, C.-W.; Shi, J.-M.; Yu, Y.; Yang, H.-B. Cross-Linked Supramolecular Polymer Metallogels Constructed via a Self-Sorting Strategy and Their Multiple Stimulus-Response Behaviors. *Chem. Commun.* **2015**, *51*, 16813–16816. (b) Dong, S.; Luo, Y.; Yan, X.; Zheng, B.; Ding, X.; Yu, Y.; Ma, Z.; Zhao, Q.; Huang, F. A Dual-Responsive Supramolecular Polymer Gel Formed by Crown Ether Based Molecular Recognition. *Angew. Chem., Int. Ed.* **2011**, *50*, 1905–1909.
- (16) (a) Okesola, B. O.; Vieira, V. M. P.; Cornwell, D. J.; Whitelaw, N. K.; Smith, D. K. 1,3:2,4-Dibenzylidene- D -Sorbitol (DBS) and Its Derivatives – Efficient, Versatile and Industrially-Relevant Low-Molecular-Weight Gelators with Over 100 Years of History and a Bright Future. *Soft Matter* **2015**, *11*, 4768–4787. (b) Draper, E. R.; Adams, D. J. Low-Molecular-Weight Gels: The State of the Art. *Chem* **2017**, *3*, 390–410. (c) Chivers, P. R. A.; Smith, D. K. Shaping and Structuring Supramolecular Gels. *Nat. Rev. Mater.* **2019**, *4*, 463–478.
- (17) (a) Badjić, J. D.; Nelson, A.; Cantrill, S. J.; Turnbull, W. B.; Stoddart, J. F. Multivalency and Cooperativity in Supramolecular Chemistry. *Acc. Chem. Res.* **2005**, *38*, 723–732. (b) Hogben, H. J.; Sprafke, J. K.; Hoffmann, M.; Pawlicki, M.; Anderson, H. L. Stepwise Effective Molarities in Porphyrin Oligomer Complexes: Preorganization Results in Exceptionally Strong Chelate Cooperativity. *J. Am. Chem. Soc.* **2011**, *133*, 20962–20969. (c) Fasting, C.; Schalley, C. A.; Weber, M.; Seitz, O.; Hecht, S.; Koksch, B.; Dernedde, J.; Graf, C.; Knapp, E.-W.; Haag, R. Multivalency as a Chemical Organization and Action Principle. *Angew. Chem., Int. Ed.* **2012**, *51*, 10472–10498. (d) Ahn, Y.; Jang, Y.; Selvapalam, N.; Yun, G.; Kim, K. Supramolecular Velcro for Reversible Underwater Adhesion. *Angew. Chem., Int. Ed.* **2013**, *52*, 3140–3144.
- (18) (a) Zhukhovitskiy, A. V.; Zhong, M.; Keeler, E. G.; Michaelis, V. K.; Sun, J. E. P.; Hore, M. J. A.; Pochan, D. J.; Griffin, R. G.; Willard, A. P.; Johnson, J. A. Highly Branched and Loop-Rich Gels via Formation of Metal–Organic Cages Linked by Polymers. *Nat. Chem.* **2016**, *8*, 33–41. (b) Zhang, Q.; Tang, D.; Zhang, J.; Ni, R.; Xu, L.; He, T.; Lin, X.; Li, X.; Qiu, H.; Yin, S.; Stang, P. J. Self-Healing Heterometallic Supramolecular Polymers Constructed by Hierarchical Assembly of Triply Orthogonal Interactions with Tunable Photophysical Properties. *J. Am. Chem. Soc.* **2019**, *141*, 17909–17917. (c) Wang, H.; Zhu, C. N.; Zeng, H.; Ji, X.; Xie, T.; Yan, X.; Wu, Z. L.; Huang, F. Reversible Ion-Conducting Switch in a Novel Single-Ion Supramolecular Hydrogel Enabled by Photoresponsive Host–Guest Molecular Recognition. *Adv. Mater.* **2019**, *31*, No. 1807328. (d) Zhang, Z.; Cheng, L.; Zhao, J.; Zhang, H.; Zhao, X.; Liu, Y.;

Bai, R.; Pan, H.; Yu, W.; Yan, X. Muscle-Mimetic Synergistic Covalent and Supramolecular Polymers: Phototriggered Formation Leads to Mechanical Performance Boost. *J. Am. Chem. Soc.* **2021**, *143*, 902–911.

(19) (a) Tan, G.; Zhong, Y.; Yang, L.; Jiang, Y.; Liu, J.; Ren, F. A Multifunctional MOF-Based Nanohybrid as Injectable Implant Platform for Drug Synergistic Oral Cancer Therapy. *Chem. Eng. J.* **2020**, *390*, No. 124446. (b) Wang, H.; Luo, Z.; Wang, Y.; He, T.; Yang, C.; Ren, C.; Ma, L.; Gong, C.; Li, X.; Yang, Z. Enzyme-Catalyzed Formation of Supramolecular Hydrogels as Promising Vaccine Adjuvants. *Adv. Funct. Mater.* **2016**, *26*, 1822–1829. (c) Gao, F.; Xie, W.; Miao, Y.; Wang, D.; Guo, Z.; Ghosal, A.; Li, Y.; Wei, Y.; Feng, S.-S.; Zhao, L.; Fan, H. M. Magnetic Hydrogel with Optimally Adaptive Functions for Breast Cancer Recurrence Prevention. *Adv. Healthcare Mater.* **2019**, *8*, No. 1900203. (d) Qi, Y.; Min, H.; Mujeeb, A.; Zhang, Y.; Han, X.; Zhao, X.; Anderson, G. J.; Zhao, Y.; Nie, G. Injectable Hexapeptide Hydrogel for Localized Chemotherapy Prevents Breast Cancer Recurrence. *ACS Appl. Mater. Interfaces* **2018**, *10*, 6972–6981.

(20) Zhou, M.; Li, L.; Li, L.; Lin, X.; Wang, F.; Li, Q.; Huang, Y. Overcoming Chemotherapy Resistance via Simultaneous Drug-Efflux Circumvention and Mitochondrial Targeting. *Acta Pharm. Sin. B* **2019**, *9*, 615–625.

□ Recommended by ACS

Molecular Barrels as Potential Hosts: From Synthesis to Applications

Ranit Banerjee, Partha Sarathi Mukherjee, et al.

MARCH 28, 2023

JOURNAL OF THE AMERICAN CHEMICAL SOCIETY

[READ ▶](#)

Selective Binding and Isomerization of Oximes in a Self-Assembled Capsule

Kuppusamy Kanagaraj, Yang Yu, et al.

MARCH 01, 2023

JOURNAL OF THE AMERICAN CHEMICAL SOCIETY

[READ ▶](#)

Solvent-Dependent Self-Assembly of a Pillar[5]arene-Based Poly-Pseudo-Rotaxane Linked and Threaded by Silver(I) Trifluoroacetate: A Double Role

Seulgi Kim, Eunji Lee, et al.

JANUARY 20, 2023

INORGANIC CHEMISTRY

[READ ▶](#)

Supramolecular Recognition within a Nanosized “Buckytrap” That Exhibits Substantial Photoconductivity

Sajal Sen, Atanu Jana, et al.

JANUARY 06, 2023

JOURNAL OF THE AMERICAN CHEMICAL SOCIETY

[READ ▶](#)

[Get More Suggestions >](#)